Mathematical Geology, Vol. 35, No. 8, November 2003 (© 2003)

Geostatistical Analysis of Inverse Problem Variables: Application to Seismic Tomography[1]

Juan L. Fernández Martínez,[2] César O. Menéndez Pérez,[2] Luis M. Pedruelo González,[2] José P. Fernández Alvarez,[3] and Pablo Cienfuegos Suárez[4]

In this article we present a geostatistical approach to the transmission tomographic inverse problem, which is based on consideration of the inverse problem variables (velocity and traveltime errors) as regionalized variables (R.V.). Their structural analysis provides us with a new method to study the geophysical anisotropy of the rock, an important source of a priori information in order to design the anisotropic corrections. The underlying idea is that the geophysical structure can be deduced from the spatial structure of the regionalized variables which result from solving the tomographic problem with an isotropic algorithm. Also, the application of the structural analysis technique to the anisotropic corrected velocity field allows us to characterize the reliability of these corrections (model quality analysis). Geostatistical formalism also provides us with different techniques (parametric and non-parametric) to estimate and even simulate the velocity in the areas where this field has been considered anomalous based on field studies and on geophysical and statistical criteria. The kriging acts as a low-pass smoothing filter for the anomalous model parameters (velocities), but is not a substitute for an adequate filtering of the outliers before the inversion. This methodology opens the possibility of considering the inverse problem variables as stochastic processes, an important feature in cases where the tomogram is to be used as a tool of assessment to quantify the rock heterogeneities.

KEY WORDS: geostatistical analysis, seismic tomography, inverse problems.

RESEARCH INCENTIVE

Tomographic inverse problems are deterministic by nature. However, the presence of inconsistent data generates artifacts in model parameters. Errors in observed data are very common in tomographic experiments, and are mainly due to acquisition problems (Dyer and Worthington, 1988) and traveltime picking errors (Pratt

[1]Received 31 October 2002; accepted 18 August 2003.

[2]Departamento de Matemáticas, Universidad de Oviedo, C/Calvo Sotelo S/N, 33006 Oviedo, Spain; e-mail: jlfm@orion.ciencias.uniovi.es

[3]Departamento de Explotación y Prospección de Minas, Universidad de Oviedo, C/Independencia, 13, 33005 Oviedo, Spain.

[4]Instituto Geológico y Minero de España, C/Matemático Pedrayes, 25, 33005 Oviedo, Spain.

and Chapman, 1992). These spurious data may cause the convergence failure of numerical algorithms. This fact may be interpreted as a randomness phenomenon introduced in the deterministic velocity field.

To explain this last assertion let us consider the continuous tomographic problem of finding $s \in S \subset L^2(\Omega)$ that satisfies the m integral equations:

$$\int_{\Gamma_i} s(x)\, dl_{\Gamma_i} = t_i, \quad i = 1, \ldots, m,$$

where $s(x)$ is the slowness model belonging to the model space S, t_i are the observed traveltime data belonging to the data space D, and Γ_i are Fermat's raypaths between each pair of sources and receivers (Berryman, 1991). To solve this problem numerically, different kinds of least-squares-like methods have been proposed (Berryman, 1991; Dines and Lytle, 1979; Gordon, 1974; Ivansson, 1986; Scales, 1987; Pratt and Chapman, 1992). The solution vector, $s(x)$, can be interpreted as the application of a deterministic transfer function T_f to the observed data $t(x)$:

$$s(x) = T_f(t(x))$$

where T_f maps the data space D into the model space S.

Because of data inconsistencies, the observed data $t(x)$ can be considered as a random variable. Thereby, this randomness phenomenon is transmitted through the deterministic filter T_f to the slowness field $s(x)$. A similar idea has been proposed by Franklin (1970), who applies the theory of stochastic processes to obtain as much information as possible from ill-posed linear problems. Also, Ivansson (1985) introduced a statistical model to take into account data randomness in the discrete linearized solution of the tomographic inverse problem.

Various state-of-the-art methods have been proposed to solve the problem of data inconsistencies: singular value decomposition, damping, and robust optimization techniques. Another possibility arises from considering a probabilistic approach of the tomographic inverse problem. This kind of methodology has been proposed by Tarantola and Valette (1982a,b), who formulated the inverse problem in a probabilistic framework, as a combination of information coming from observed data, a priori information, and theoretical information (physics of the problem). This approach to nonlinear inverse problems also has the properties of uniqueness and consistency.

In this paper, we present a geostatistical analysis of the transmission tomographic inverse problem variables, applying this formalism to a crosshole data set acquired in an area with granitic geology: the Grimsel test site – field 1 (NAGRA, the Swiss National Cooperative for the disposal of Radioactive Waste). One of the main difficulties in this approach is to select the random variables (R.V.), as the original data (seismic traveltimes) are associated with the Fermat raypaths that are

not defined on a grid and are generally unknown. To overcome this problem, we first solve the inverse problem and consider as R.V. the velocity field and traveltime errors calculated by the inversion algorithm in the last iteration. This methodology is applied to the anisotropic and anisotropy-corrected velocity fields, providing us important sources of a priori geophysical information (structural and model quality analysis), opening the possibility of considering the inverse problem variables as stochastic processes, which is an important feature in the cases where the tomogram is to be used as a tool of assessment.

SYNTHETIC MODELING AND ANISOTROPY DETECTION

It is worth explaining that in what follows the term anisotropy has a dual sense: while the geostatistical anisotropy concerns the spatial structure of the velocity field, the geophysical anisotropy has to be interpreted as the angular dependence of the velocity field deduced from 2D tomographic sections.

As mentioned before, the basic idea to characterize the direction of geophysical anisotropy is that anisotropy is implicit in the spatial structure of the regionalized variables which result from solving the tomographic problem with an isotropic algorithm (without taking into account the anisotropic corrections). To prove this, we have generated two different synthetic anisotropic models and we performed structural analysis (variogram surface calculation). The variogram surface is perhaps the most effective technique for detecting anisotropy in the pattern of spatial continuity of a R.F. This spatial tool is also used to determine the preferential directions in which directional variograms should be calculated. In this case we are not interested in performing a classical structural analysis, we simply want to show that a rough characterization of the spatial structure of the anisotropic velocity field can help us to detect the geophysical anisotropy of the rock.

Figure 1 shows two different synthetic velocity fields and their corresponding experimental variogram surface. It can be seen that the direction of maximum correlation distance coincides with one of the main directions of geophysical anisotropy (minimum velocity in this case). Thus, the conclusion is that structural analysis of the anisotropic velocity field is a simple method to detect the main directions of geophysical anisotropy.

GEOSTATISTICAL ANALYSIS OF THE GRIMSEL DATA SET

To illustrate this technique with real data, we apply the geostatistical methodology to the Grimsel crosshole data set – field 1 (Gelbke, Miranda, and Sattel, 1989). The geometry of the survey is approximately rectangular bounded by two

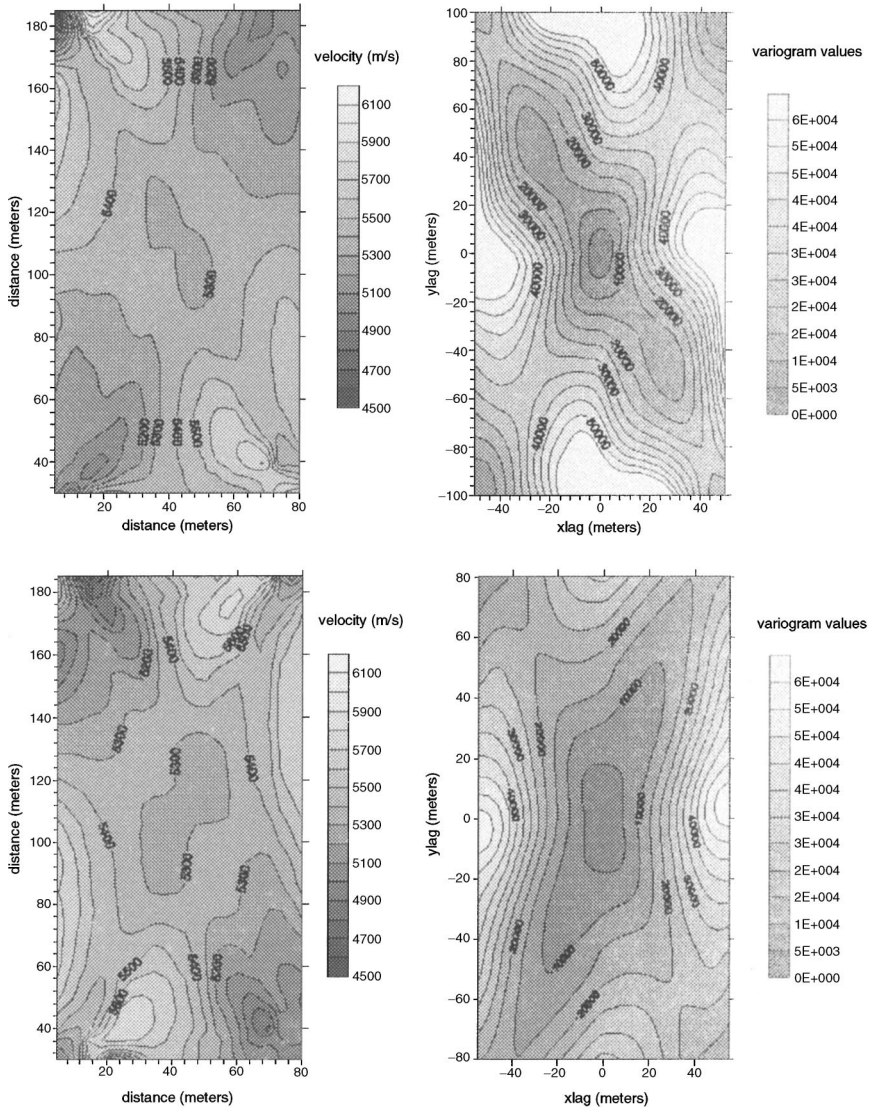

Figure 1. Two different synthetic anisotropic models (tomograms) and their corresponding experimental variogram surfaces. A rough characterization of their spatial structure (covariance models) serves to delineate the direction of geophysical anisotropy.

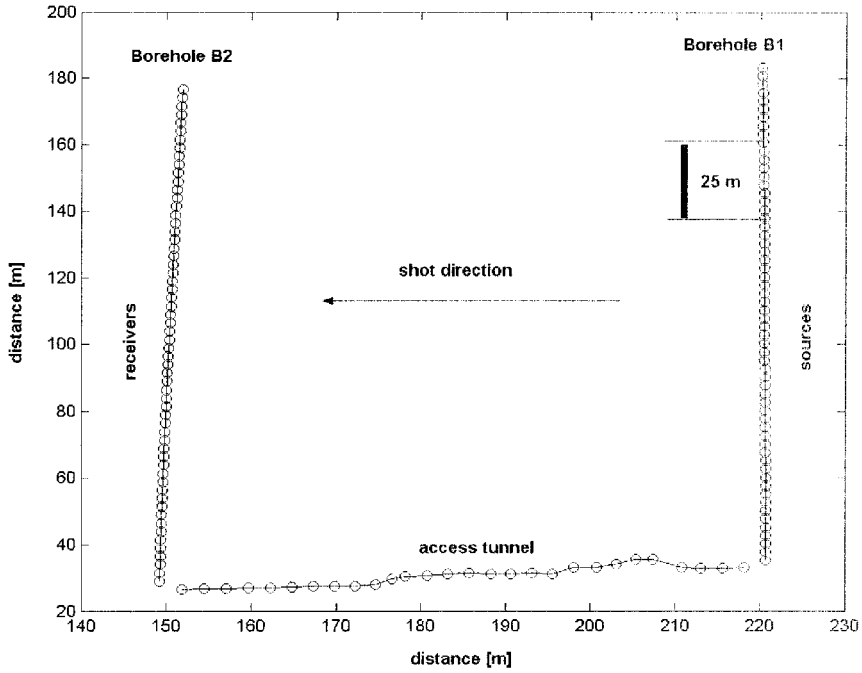

Figure 2. Grimsel data set 1. The acquisition survey is composed of two "parallel" boreholes: B1 (sources) and B2 (receivers).

boreholes (B1 and B2). The dimensions of the granitic domain are 70 $\times$ 140 m. The survey is composed of 58 sources and 60 receivers separated by a distance of 2.5 m (Fig. 2).

Several research groups have inverted this data set. Gelbke, Miranda, and Sattel (1989) studied the main sources of data errors: (systematic errors due to acquisition problems, time shifts caused by the filtering techniques, etc.,) and estimated the degree and direction of geophysical anisotropy using velocity versus azimuth plots. From this angular dependence they concluded that the granite can be modeled by a weak transverse elliptical anisotropy given by the parameters:

$$\beta = N30^{\circ}W, \qquad \lambda = \frac{V_{\max} - V_{\min}}{V_{\max}} = 3\%,$$

where β and λ stand for the direction (the angle that maximum velocity, $V_{\max}$, forms with the borehole direction measured counterclockwise) and the ratio of anisotropy. These parameters are used in the tomographic algorithm to account

for the anisotropic corrections. These earlier studies have been updated by Albert and others (1998). Maurer and Green (1997) used a coupled inverse method, well known in earthquake studies, to investigate the effects of coordinate misallocation and weak anisotropy in the tomographic images for this granitic rock. The presence of outliers in the data set created some artifacts in the velocity field (large range of apparent P wave velocities).

Geostatistical Modeling of Anisotropic Velocities: Anisotropy Detection

The main R.V. is the anisotropic velocity field (Fig. 3(A)) which results from solving the discrete linearized inverse problem in a rectangular grid of 3.1×3.1 m cells. To facilitate anisotropy detection we also consider as a secondary R.V. the traveltime errors (Fig. 3(B)) calculated by the inversion code in the last iteration of the numerical algorithm when the RMS error tolerance is reached.

Figure 4 shows the histogram and the graphical plot of normality of the anisotropic velocity field. The mean (5.15 $km{\cdot}s^{-1}$) and the median (5.17 $km{\cdot}s^{-1}$) are very similar and the statistical distribution of velocity is close to a Gaussian distribution. The range of variation is 4.7–5.6 $km{\cdot}s^{-1}$. The normality plot shows that model parameters can be considered close to normal behavior in the range 4.7–5.80 $km{\cdot}s^{-1}$. This interval is consistent with the geological and geophysical studies

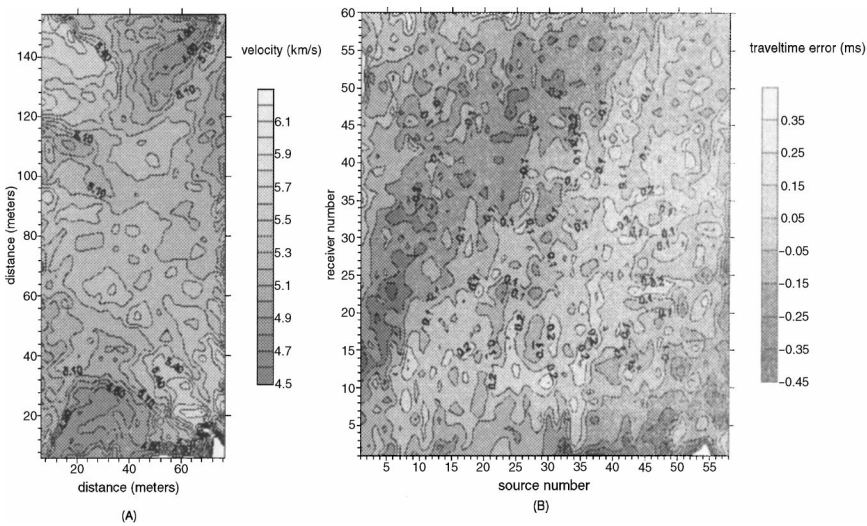

Figure 3. Anisotropic random variables used in the geostatistical analysis for anisotropy detection: (A) anisotropic velocity field ($km{\cdot}s^{-1}$); (B) traveltime errors (ms). The direction of the geophysical anisotropy can be deduced from the geostatistical analysis of their respective covariance models.

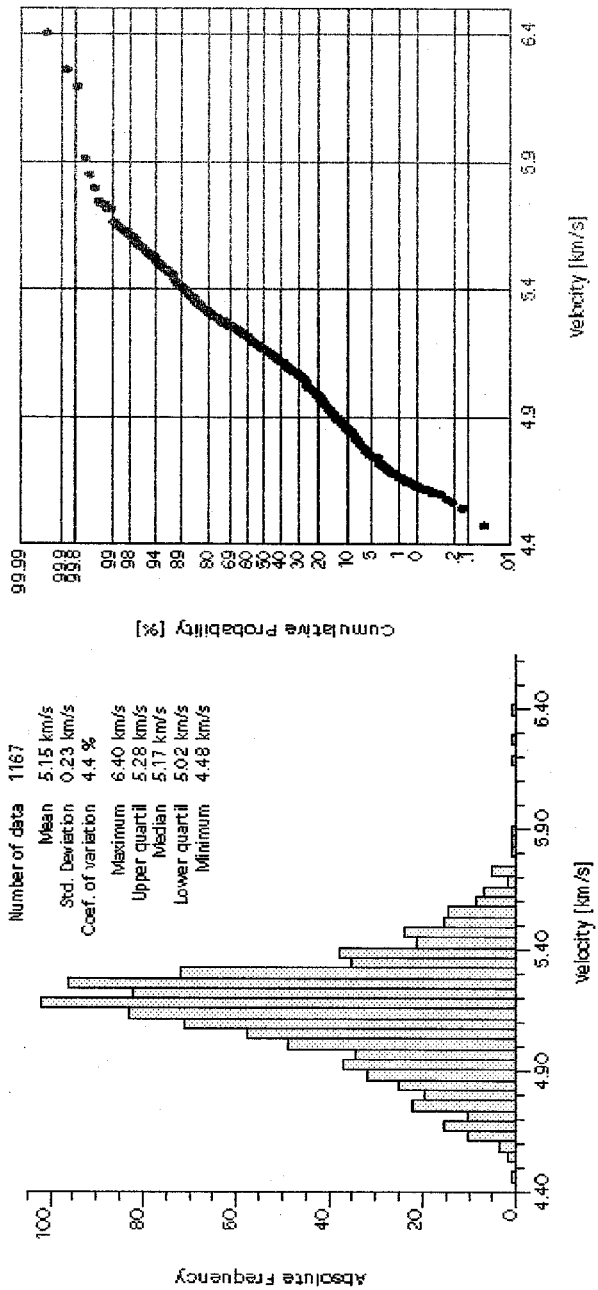

Figure 4. Histogram and normality plot of the anisotropic velocities. Inversion-generated velocities are in the range 4.48–6.40 km·s^{-1}. The statistical distribution of velocity is close to a Gaussian distribution. The normality plot shows that velocities can be considered close to normal behavior in the range of 4.70–5.80 km·s^{-1}.

undertaken in the granitic massif (Albert and others, 1998; Gelbke, Miranda, and Sattel, 1989). Therefore it is possible to conclude that statistical analysis allows us to unravel the presence of different statistical populations and to determine the range of normal model parameters, i.e., the areas where velocity has been correctly estimated.

In this case, prior to the structural analysis we have performed a normal score transformation of the R.V., becuase the kriging estimator provides an optimum result if the R.F. has a normal distribution.

Figure 5(A) shows the experimental variogram surface of the anisotropic velocity field. As can be seen, the maximum range (correlation distance) occurs in the N30°–40°W and does coincide with the direction of weak transverse elliptical anisotropy revealed by previous geophysical studies (Gelbke, Miranda, and Sattel, 1989). Nevertheless there is a shorter spatial correlation in the northeast direction (N30°E), which has not been modeled. This second spatial structure motivates an extravariability (higher sill) of the variograms inferred in the north to east directions. These structures could be related to a system of faults (NW directions) and intrusions (NE directions) which are approximately orthogonal (Gelbke, Miranda, and Sattel, 1989). The omnidirectional variogram of this R.F. corresponds to a spherical model with a range of 50 m, a sill (statistical variance) of 0.65 with a nugget effect contribution (microvariabilities) of 0.10. The directional variograms obtained on the basis of structural analysis focusing on the main directions of anisotropy showed that the fitted theoretical model is spherical with a maximum range of 60 m N34°W, a minimum range of 36 m N56°E, and a sill of 0.57 (with a nugget contribution of 0.10).

The main conclusion of this analysis is that geophysical anisotropy is implicit in the spatial structure of the anisotropic velocity field. The direction of geophysical anisotropy can be detected using structural analysis of this R.V. Nevertheless the geostatistical anisotropy ratio does not coincide with the geophysical anisotropy ratio. This is understandable as both parameters describe different phenomenon.

To confirm the results of the anisotropy detection we have also used the traveltime errors in the last iteration of the numerical algorithm (Fig. 3(B)), focusing on the areas where the calculated errors are most significant (sources: 10–40, receivers: 10–40). Figure 5(B) shows the experimental variogram surface for this secondary R.V. The direction of maximum error correlation is defined by the line between sources and receivers of equal number, which is approximately N30°E. The direction of minimum error correlation (N30°W) coincides with the direction of geostatistical anisotropy unraveled by the structural analysis of the anisotropic velocity field. The correlogram in this direction shows that errors are correlated within a distance of 38 m (15 sources or receivers) and, as expected, the variogram shows a larger contribution of the nugget effect (60% of the statistical variance or sill).

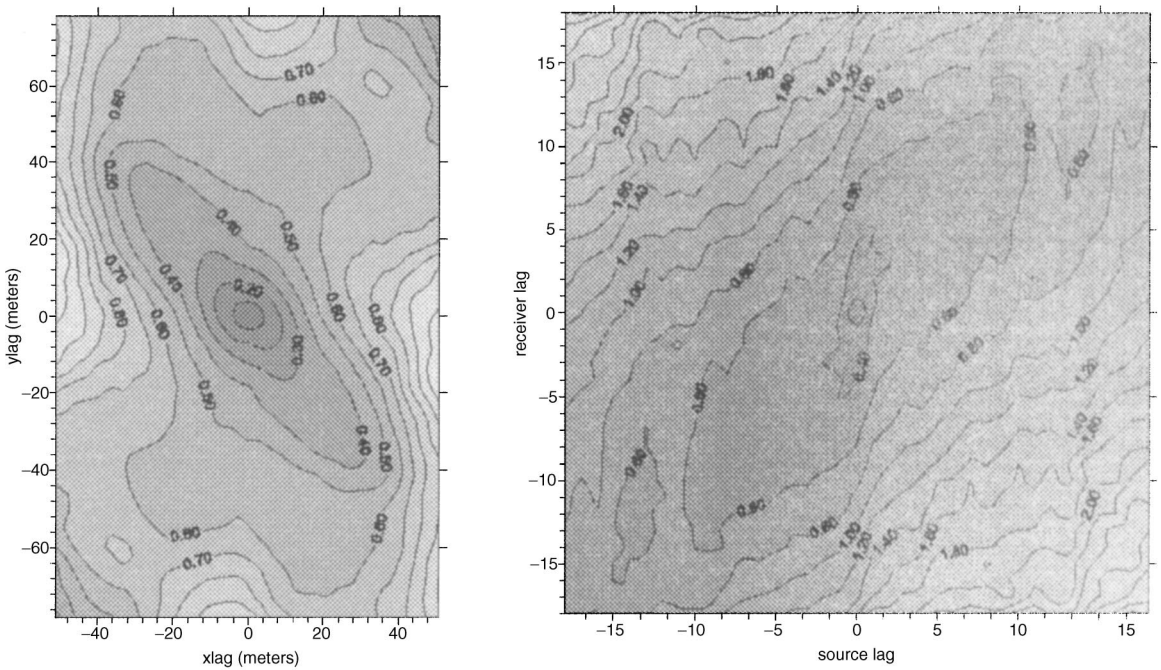

Figure 5. (A) Experimental variogram surface of the anisotropic velocity field. The maximum range occurs in the direction N30°–40°W and does coincide with the direction of weak transverse elliptical anisotropy revealed by previous geophysical studies. The variogram surface also shows the existence of a secondary, shorter spatial correlation in the northeast direction (N30°E). (B) Experimental variogram surface of anisotropic traveltime errors. The direction of minimum error correlation (N30°W) does coincide with the direction of geostatistical anisotropy revealed by the structural analysis of the anisotropic velocity field.

Geostatistical Modeling of Anisotropy-Corrected Velocities: Model Quality Analysis

Using a SIRT (Simultaneous Iterative Reconstruction Technique; Dines and Lytle, 1979) algorithm we have inverted the traveltime data on a 3.1 × 3.1 m grid, applying the anisotropy correction given by the elliptical model deduced by Gelbke, Miranda, and Sattel (1989) from geophysical studies. As we have shown, this model of geophysical anisotropy has also been confirmed by structural analysis of the anisotropic velocity field.

Figure 6(A) and (B) shows the velocity field corrected from anisotropy (isotropic velocity) and the corresponding traveltime errors. It is important to note that an adequate anisotropic correction will cause the isotropic velocity field to exhibit an isotropic covariance model and the traveltime errors to show up as a white noise or at least as a notable decrease in terms of spatial correlation distance.

Figure 7(A) shows the experimental variogram surface of the anisotropy-corrected velocity. The pattern of spatial continuity of this variable is very complicated, and can be described as an isotropic R.V. in the shorter ranges (less than 35 m). For longer ranges the influence of two nested structures in the northwest and northeast directions can be observed, which are due to the anisotropic correction. Figure 7(B) shows the variogram surface model obtained with these three nested structures. The first spatial structure has a range of 35 m and corresponds to the isotropic feature identified in the variogram surface. The other nested structures makes the R.V. zonal anisotropic, since spatial correlation in these models only takes place in their respective directions (N25°E and N68°W). The directional variograms showed that the fitted theoretical model corresponds to an isotropic spherical model with a range of 32 m and a sill of 0.95 (with a nugget effect contribution of 0.07).

Figure 8 shows the experimental variogram surface for anisotropy-corrected traveltime errors, focusing on the areas where those are the largest (sources: 20–60, receivers: 20–60) (Figure 6B). Errors still show a spatial correlation that has decreased to 5 m (a pair of sources or receivers) instead of 38 m, which was the correlation distance in the case of the anisotropic traveltime errors.

Therefore, the structural analysis of the R.V. obtained by solving the transmission tomographic problem with an isotropic algorithm (taking into account the anisotropy correction) can be used to characterize the reliability of these corrections. Also, from this analysis we infer a spatial model (covariance model) which is going to be used in the kriging and in the conditional simulation stages.

To filter the anomalous features present in the isotropic velocity field we have estimated this R.V on a finer grid (2.5 × 2.5 m) by means of ordinary kriging, using as available information the isotropic velocity field, which is defined in a coarser grid (3.1 × 3.1 m). The grid has been changed for filtering purposes, since

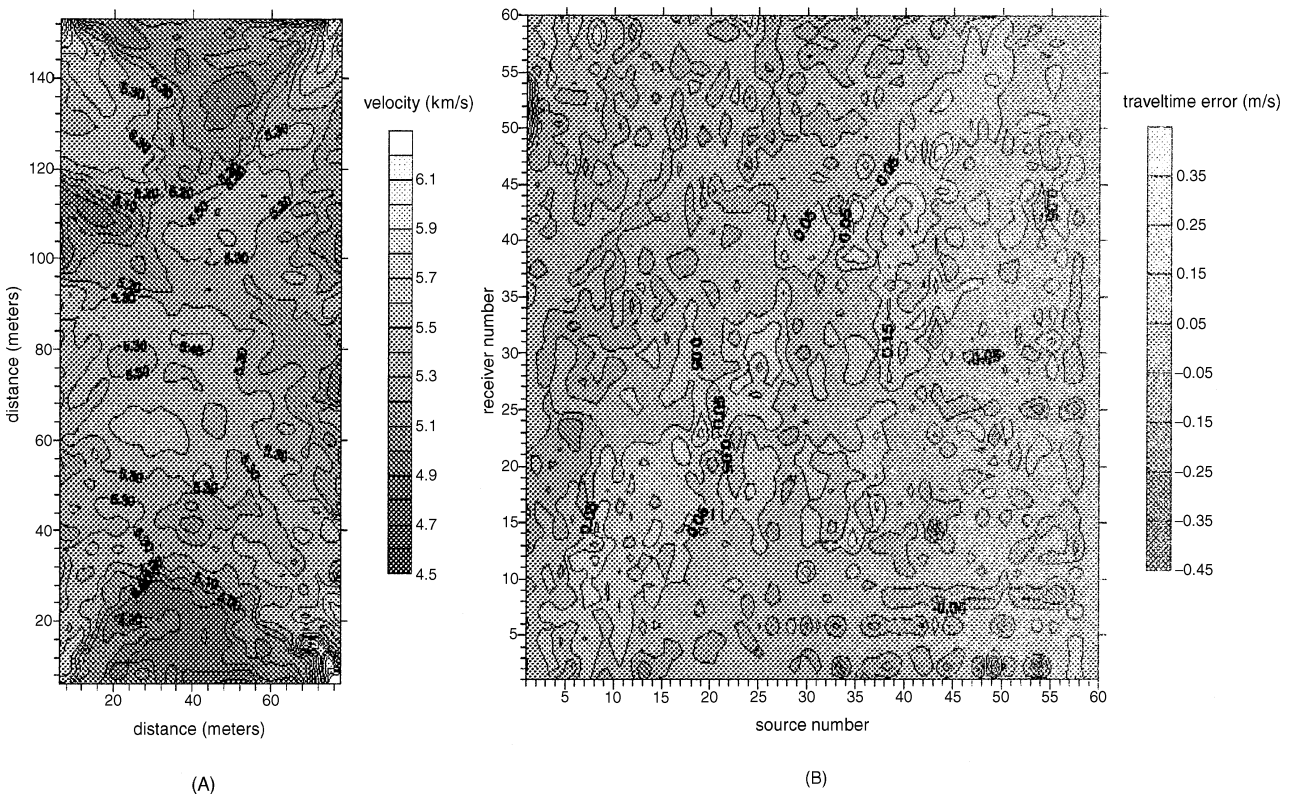

Figure 6. Anisotropy-corrected (isotropic) velocity field and associated traveltime errors. An adequate anisotropic correction will cause the isotropic velocity field to show an isotropic covariance model and the traveltime errors to show up as white noise.

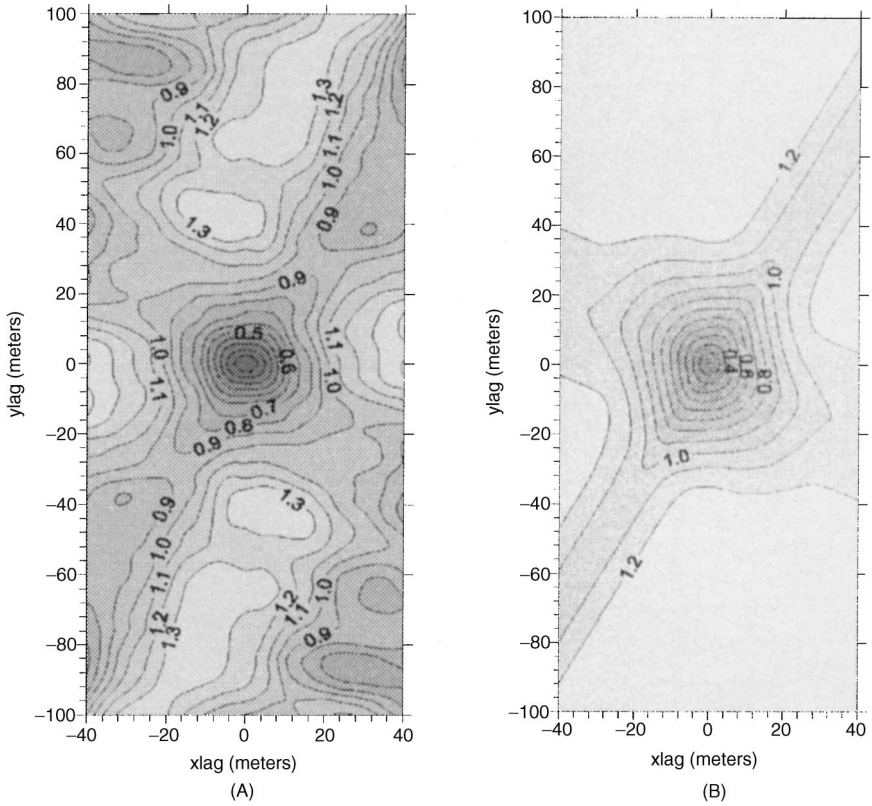

Figure 7. Experimental and model variogram surface of the anisotropy-corrected velocity. This R.V. can be considered isotropic in the shorter ranges (less than 35 m). For longer ranges the influence of two nested structures in the northwest and northeast directions (due to the anisotropic correction) can be seen.

kriging is an exact estimator, i.e., the estimated field will pass through the available infomation (velocity values on the original grid). As a pattern of spatial continuity we adopted an isotropic spherical model with a range of 35 m, a sill of 0.95, and a nugget effect of 0.10, inferred by means of a classical variography.

Figure 9(A) and (B) shows the ordinary kriging tomogram and the indicator kriging probability field for a cutoff of 5.0 km·s^{-1}. As one can see, the spatial structure of the isotropic velocity field (Fig. 6(A)) has been conserved in the ordinary kriging velocity field (Fig. 9A), but the high anomalies in the corners of the original R.V. (isotropic velocity field) have been suppressed. Also, the velocity range of variation of the ordinary kriging field, 4.8–5.6 km·s^{-1}, is consistent with the geological and geophysical studies. As expected, kriging acts as a low-pass smoothing filter for the anomalous model parameters. In the indicator kriging

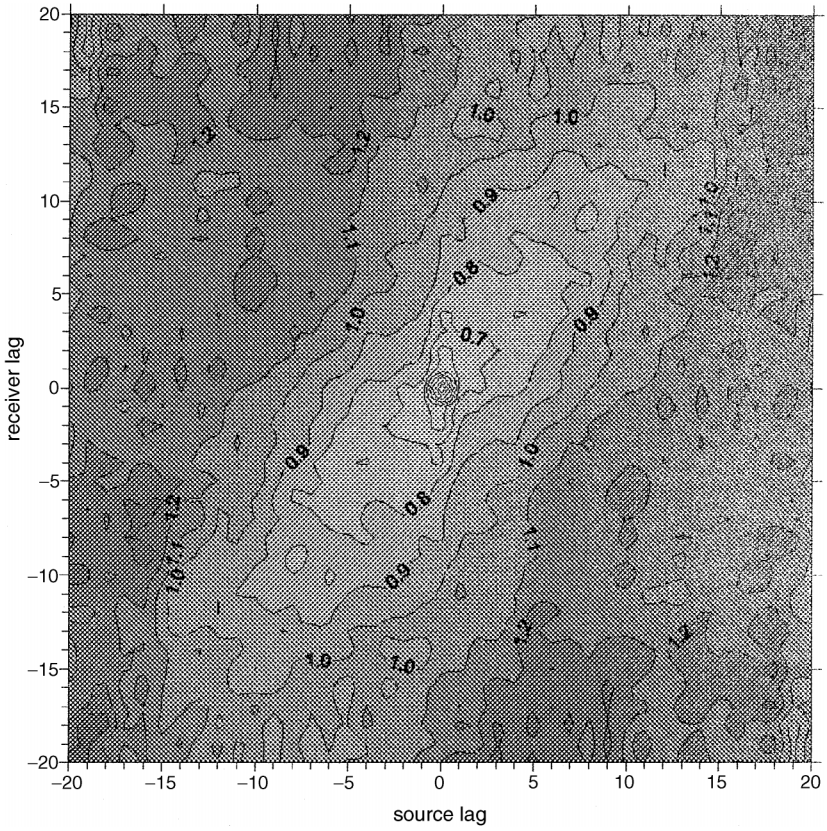

Figure 8. Experimental variogram surface for anisotropy-corrected traveltime errors. Errors still show a spatial correlation that has decreased to 5 m instead of 38 m, which is the correlation distance in the case of the anisotropic traveltime errors. This analysis serves to confirm the reliability of the anisotropic correction.

field (Fig. 9(B)) the areas with higher probability (close to 1.0) delimit in the tomogram the low velocity zones. This knowledge is important for the detection and probabilistic classification of the break zones in a geotechnical study. Thus, the kriging techniques (parametric and nonparametric) serve to estimate the velocity field in the areas where this field has been considered anomalous and to quantify the uncertainty of these estimations. The results shown in Figure 9(A) can be improved by an adequate filtering of the outliers. If we consider a filtered data set, the final result is slightly different: the north velocity field has a larger spatial range towards the south. This conclusion is in agreement with results showed in Gelbke, Miranda, and Sattel (1989). It is also important to note that these authors used a complete angular coverage of the massif (three-ray data sets) while in our study

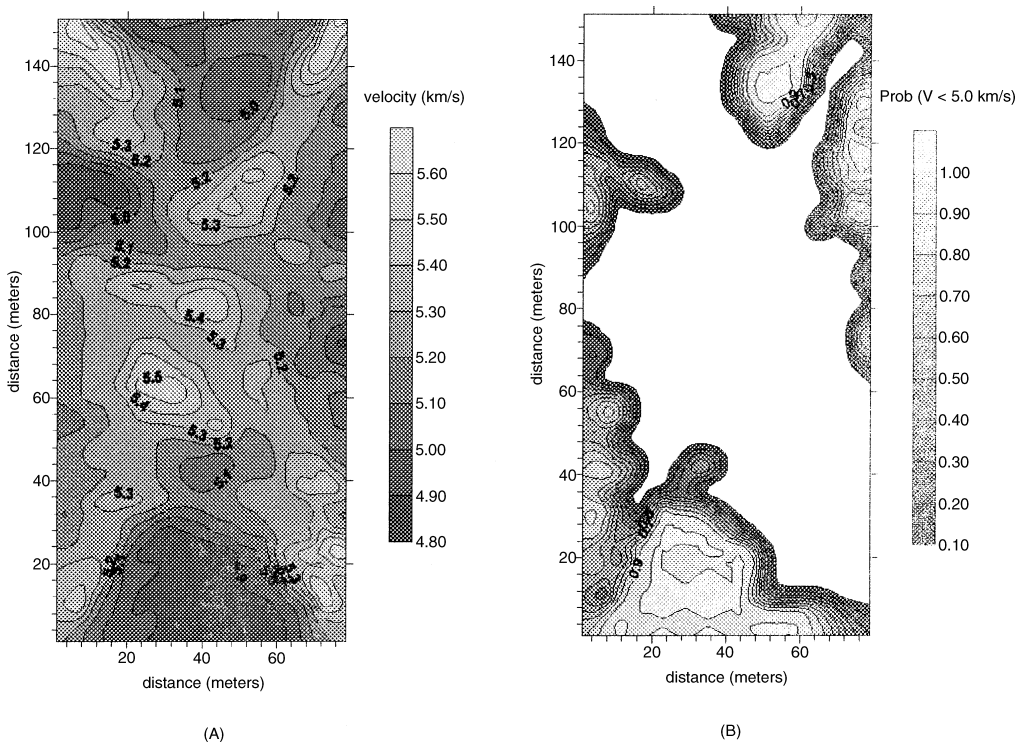

Figure 9. (A) Ordinary kriging of the isotropic velocity field in a 2.5 × 2.5 m grid, obtained using an isotropic spherical model with a range of 35 m. The spatial structure of the isotropic velocity field has been conserved, but the high velocity anomalies have been suppressed. (B) Indicator kriging of the isotropic velocity field for a cutoff of 5.0 km·s^{-1}. The areas with higher probability delimit in the tomogram the break zones.

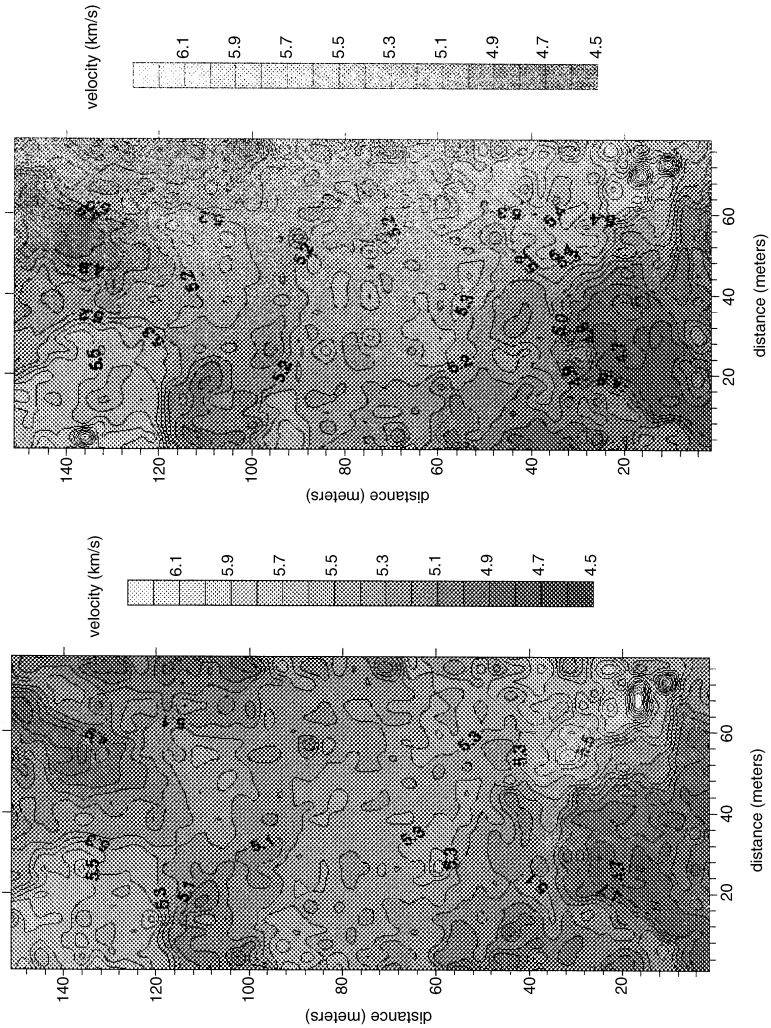

Figure 10. Two of the infinity equiprobable conditional simulations of the isotropic velocity field obtained via the sequential Gaussian simulation algorithm. The conditional simulation technique reproduces a similar spatial structure to the original isotropic velocity field and emphasizes the R. V. heterogeneities smoothed by the kriging estimator.

we only worked with one of these (data set 1). An important conclusion is that the kriging filter does not substitute an adequate filtering of the outliers previous to the inversion process. This is understandable since geostatistics does not create new information.

Finally, the geostatistical methodology provides a powerful tool (conditional simulation techniques) to study and quantify the massif heterogeneities. Tomogram simulation is very important when these are used to generate plausible geological models. This is the case in hydrogeological models for contaminant migration, where the tomogram is used to infer the geology and the permeability field. The aim of these models is to estimate the contaminant paths. These paths depend nonlinearly on the hydrogeological parameters and, thus, simulation techniques are needed. The use of kriging fields to estimate fluid paths will lead the models to give an incorrect solution, because they are highly dependent on the maximal and minimal values of permeability. Figure 10 shows two different conditional simulations of the isotropic velocity, obtained via the sequential Gaussian simulation algorithm (Deustsch and Journel, 1992) applied to the normal-score-transformed R.V. (isotropic velocity field). As expected, the conditional simulation technique reproduces a similar spatial structure to the original isotropic field and emphasizes the R.V. heterogeneities smoothed by the kriging estimator.

As a main conclusion, the geostatistical methodology opens the possibility of considering the inverse problem variables as stochastic processes, an important feature in cases where the tomogram is to be used as a tool of assessment.

CONCLUSIONS

In this paper we have focused our attention on showing that the geostatistical methodology is well suited to the probabilistic analysis of the deterministic velocity field generated by inversion. The geostatistical analysis of these variables (anisotropic and isotropic velocities and travcltime errors) provides us with a new method for inferring crucial information about model parameters in seismic tomographic experiments (range of normal velocities and direction of the geophysical anisotropy) and can be considered as a quality analysis tool to characterize the reliability of the anisotropy corrections incorporated into the numerical [algorithm]. These are important sources of a priori information for the numerical algorithms to solve the tomographic inverse problem. Also, kriging techniques act as a filter for the anomalous model parameters and serve to quantify the uncertainty of these estimations. Finally, the geostatistical approach to inverse problems opens the way to the application of nonparametric kriging and conditional simulation techniques to the model parameters (velocity field), which are very useful in cases where the tomogram is to be used as a tool of assessment to quantify probabilistically the rock heterogeneities.

ACKNOWLEDGMENTS

We thank NAGRA (the Swiss National Cooperative for the Disposal of Radioactive Waste) for giving us the permission to use the Grimsel data set (data set 1 – field 1) to illustrate this technique, Dr B. C. Dyer for providing us with a copy of his inversion code (DIVINE), and Dr Sergei Schmarev (Dept. of Mathematics, University of Oviedo) for constructive reviews of this manuscript.

REFERENCES

Albert, W., Buhnemann, J., Holliger, K., Maurer, H., Pratt, R., and Stekl, I., 1998, Grimsel test site: Further development of seismic tomography: Nagra technical report NTB 97–05, 120 p.

Berryman, J. G., 1991, Lectures notes on nonlinear inversion and tomography. Borehole seismic tomography: Technical report, Lawrence Livermore National Laboratory, 134 p.

Deustsch, C. V., and Journel, A. G., 1992, GSLIB. Geostatistical Software Library and User's Guide: Oxford University Press, Oxford, 340 p.

Dines, K. A., and Lytle, R. J., 1979, Computerized geophysical tomography: IEEE Proc., v. 67-7, p. 1065–1073.

Dyer, B. C., and Worthington, M. H., 1988, Some sources of distortion in tomographic velocity images: Geophys. Prospect., v. 36, p. 209–222.

Franklin, J. N., 1970, Well-posed stochastic extensions of ill-posed linear problems: J. Math. Anal. Appl., v. 31, p. 682–716.

Gelbke, C., Miranda, F., and Sattel, G., 1989, The results of a seismic transmission tomography survey at the Grimsel rock laboratory: The log Analyst, July–August, p. 243–260.

Gordon, R., 1974, A tutorial on ART: IEEE Trans. Nucl. Sci., NS-21, p. 78–93.

Ivansson, S., 1985, A study of methods for tomographic velocity estimations in the presence of low-velocity zones: Geophysics, v. 50-6, p. 969–988.

Ivansson, S., 1986, Seismic borehole tomography: Theory and computational methods: IEEE Proc., v. 74-2, p. 328–338.

Maurer, H., and Green, A. G., 1997, Potential coordinates mislocations in crosshole tomography: Results from the Grimsel test site, Switzerland: Geophysics, v. 62-6, p. 1696–1709.

Pratt, R. G., and Chapman, C. H., 1992, Traveltime tomography in anisotropic media: Geophys. J., v. 109, p. 20–37.

Scales, J. A., 1987, Tomographic inversion via the conjugate gradient method: Geophysics, v. 52, p. 179–185.

Tarantola, A., and Valette, B., 1982a, Inverse problems = Quest for information: J. Geophys., v. 50, p. 159–170.

Tarantola, A., and Valette, B., 1982b, Generalized nonlinear inverse problems solved using the least squares criterion: Rev Geophys. Space Phys., v. 20, p. 219–232.